38

NASA Technical Paper 1344

Thermal Characteristics of the 12-Gigahertz, 200-Watt Output Stage Tube for the Communications Technology Satellite

Arthur N. Curren

OCTOBER 1978

NASA

NASA Technical Paper 1344

Thermal Characteristics of the 12-Gigahertz, 200-Watt Output Stage Tube for the Communications Technology Satellite

Arthur N. Curren
Lewis Research Center
Cleveland, Ohio

National Aeronautics
and Space Administration

**Scientific and Technical
Information Office**

1978

SUMMARY

A description of the methods used to measure component temperatures and heat-rejection rates in a simulated space environment on candidate output stage tubes (OST's) developed for the Communications Technology Satellite is presented along with summaries of experimentally determined values. The OST's were operated over the entire anticipated operating drive range from the dc beam (zero drive) condition to the 6-decibel overdrive condition. The baseplate temperature was varied from -10° to 58° C with emphasis placed on the testing done at 45° C, the normal anticipated operating temperature. The heat-rejection rate of the OST baseplate ranged from 7.6 watts at the dc beam condition to 184.5 watts at the 6-decibel overdrive condition; the heat-rejection rate of the multistage depressed collector (MDC) cover ranged from 192.2 to 155.9 watts for the same conditions. The maximum OST temperature measured on the MDC cover was 227° C during a dc beam test. The minimum temperature measured, also on the MDC cover, was -67.5° C at the end of an extended simulated eclipse test period. No effects were observed on the OST thermal characteristics due to vibration testing or temperature-reversal cycle testing.

INTRODUCTION

The Communications Technology Satellite (CTS), developed jointly by NASA and the Canadian Department of Communications, was launched into a geostationary orbit in January 1976. The launch vehicle, a three-stage Thor Delta model 2914, placed the satellite on station in an equatorial orbit at 116° west longitude at an altitude of about 35 887 kilometers (22 300 miles). From this position, just west of South America, CTS broadcasts in a newly allocated satellite frequency band (12 GHz) to Canada and the United States, including Alska. New technology has increased the CTS transmitting power level up to 20 times that of earlier satellites. This increased power permits television reception and two-way voice communication with relatively inexpensive ground equipment in the areas served. The satellite is being used to demonstrate new technology and to conduct communication experiments that are concerned with satisfying the needs of various segments of society. The communication experiments include programming related to technology, education, medicine, business, emergency services, and ratio and television services (ref. 1).

The CTS output stage tube (OST) is a travelling-wave-tube amplifier designed to

have a saturated radiofrequency (rf) output power of about 200 watts at a frequency of 12 gigahertz and an overall efficiency of more than 40 percent. The interaction portion (body) of the OST is mounted inside the spacecraft to a platform fitted with variable conductance heat pipes that transfer most of the rejected heat to a remote radiating surface. The collector portion of the OST protrudes from the spacecraft to dissipate heat at a relatively high temperature directly to space. The experimental investigation described in this report was performed because the design of the spacecraft radiating surfaces and the heat pipe system is strongly influenced by the thermal characteristics of the OST. Prior to this investigation, the spacecraft thermal control system design included heat-rejection-rate estimates for the OST body that proved to be significantly lower than the actual values determined by the experiments. On the basis of the results of the early phases of these experiments, the spacecraft thermal control system was redesigned and extended to include the heat pipe system.

The measured OST thermal characteristics presented in this report can not be accurately calculated from rf and electrical performance measurements. Furthermore, a review of the open literature revealed no applicable experimental studies on which to base reliable estimates of the required CTS OST thermal characteristics. Consequently, since the experimental methods employed in this study proved to be quite effective, a moderately detailed description of the experimental method is included herein along with thermal characteristic result summaries as a reference for similar applications.

APPARATUS AND EQUIPMENT

Output Stage Tube

The output stage tube (OST) for the Communications Technology Satellite (CTS) is a 12-gigahertz, 200-watt, coupled-cavity travelling wave tube that uses periodic permanent-magnet focusing. The tube was manufactured by the Electron Tube Division of Litton Industries, Inc., San Carlos, California. A photograph of one of the OST's produced for this program is shown in figure 1. This OST is similar to the flight unit configuration. The major components of the tube are indicated in the figure.

The portion of the OST indicated as the body in figure 1 consists of an electron gun, an rf-interaction section, and a refocusing section. These components are shown in more detail in the cutaway drawing in figure 2. Figure 2 also shows schematically the configuration of the multistage depressed collector (MDC) portion of the OST. Details of the design and application criteria for developing the OST, as well as a rigorous treatment of its operation, are given in references 2 to 6. It is sufficient here to indicate that in OST operation electrons pass from the electron gun through the rf interaction section and refocusing region to the MDC where they were collected selectively by

energy levels with relatively little heat release. From the MDC the electrons are returned to the cathode through an external power supply. This method of electron return to the cathode enhances the OST overall electrical efficiency.

In addition to electron gun resistance heating, heat is generated within the OST body by electron beam interception with the coupled-cavity ferrule tips and by sever losses and cavity skin-effect losses. Heat is generated in the MDC by the electron beam impinging on the collector plates. A thermal barrier system located between the MDC assembly and the tube body minimizes the heat transfer between the two OST sections. The barrier consists of a copper radiation shield positioned between the ground-potential MDC collector plate and support flange, a tortuous thermal path (bellows) on the MDC container external surface, and thin-wall collector-stack support posts made of tubular stainless steel. These features are indicated in figure 2.

After it has been fabricated, processed, and checked out, the OST is packaged for use. The tube body is cradled in aluminum saddle blocks near the input and output waveguide ports. These saddle blocks are bolted to the OST aluminum baseplate. Indium foil shims are used to enhance heat transfer between the tube body and aluminum saddle blocks and the saddle blocks and aluminum baseplate. This arrangement is shown schematically in figure 3. Finally, a box truss and bracket packaging structure (shown in fig. 1) is attached to provide support for the collector assembly, ion pumps, and input and output waveguides.

For mission operation, the OST body is mounted inside the CTS spacecraft to a platform that is fitted with the evaporator section of a variable-conductance heat pipe array. The heat pipes are designed to transfer heat from the tube body to a radiator surface while maintaining the body temperature at a safe structural level. The MDC, however, protrudes from the spacecraft enclosure and radiates heat directly to space at a relatively high temperature. The MDC exterior surface, which will be referred to as the MDC cover in this report, was coated with SP-101 White (a paint product of the Sperex Company, Los Angeles, California) to enhance thermal radiation. Applied to a representative substrate sample, this coating was found to have a thermal emittance of about 0.9 in normal room condition spectrophotometer tests at Lewis Research Center.

Experimental determinations of the heat-rejection rates of five different CTS OST's were performed during this investigation. In addition, one of the OST's was retested after a significant modification. Because of the unique characteristics of each of the tubes and the specific purpose of the tests performed, each testing sequence was different. For the same reasons, each OST had a different instrumentation array. A schematic of the OST showing the typical thermal instrumentation used is presented in figure 4. The four thermistors shown in the figure were installed on each of the OST's by the tube supplier. Table I gives the locations of the thermal instrumentation.

Copper-constantan thermocouples (ANSI symbol T) were used for temperatures ex-

pected to be up to about 200° C (392° F), and Chromel-Alumel thermocouples (ANSI symbol K) were used for higher temperatures. The thermocouple assemblies were fabricated from 24-gage (5.1×10^{-4} m (0.0201 in.) diam) Teflon-insulated wires and were installed grounded to the OST. The reference junction temperature was oven controlled at 65.6° C (150° F). In most cases, the thermocouples were attached to the OST by a silver-loaded epoxy cement (Eccobond 56C/Catalyst 9, products of Emerson and Cuming, Inc., Canton, Mass.). Where convenient, some thermocouples were spot-welded to small stainless-steel washers and placed under existing screws on the tube packaging frame.

Thermal-Vacuum Test Facility

The major component of the CTS OST thermal-vacuum test facility (TVTF) is a horizontally mounted vacuum vessel approximately 1.83 meters (6 ft) in length by 1.22 meters (4 ft) in diameter. The vessel walls are equipped with appropriate vacuum system feed-through fittings for required instrumentation and rf, electrical, and coolant line connections. The vessel is equipped with sorption and vac-ion pumps for fore and primary puming functions, respectively. The pumping capability of the facility is such that a pressure less than 1.33×10^{-3} newton per square meter (1×10^{-5} torr) can be maintained during OST testing. Attached electric heaters permit vacuum bakeout temperatures up to 200° C with the OST removed. In addition to the thermal characteristics measuring equipment that will be described in the following sections of this report, other accessory facility equipment includes an rf driver and appropriate rf test instruments. Basic rf and electrical performance data and all thermal data are recorded by a high-speed scanning analog to digital converter system.

A schematic diagram of the TVTF with an OST in the testing position is shown in figure 5.

OST baseplate calorimeter. - A thermally isolated aluminum calorimeter, to which the OST baseplate is attached, is mounted inside the TVTF vacuum vessel (fig. 6). The OST baseplate was attached, as in the flight configuration, by the liquid silicone rubber RTV-11 (product of the General Electric Company). This calorimeter, which simulates the mounting platform of the OST in the CTS spacecraft, is used to measure the heat rejected from the body portion of the tube. The internal silicone-fluid flow system of the calorimeter was formed by an arrangement of interconnecting drilled holes. This arrangement was designed to maintain relatively uniform tube baseplate temperatures. The temperature of the silicone fluid, and consequently the baseplate, is regulated by a closed-loop heat-exchanger system located outside the vacuum vessel. As indicated in figure 4, the temperature at the OST baseplate-calorimeter interface is measured by two thermocouples. The silicone fluid (Dow Corning 200 Fluid, 5-cS viscosity, a

product of Dow Corning Corporation, Midland, Michigan) selected had compatible flow and thermal properties for the range of temperatures to be experienced in this investigation. The heat-rejection rate of the OST body was determined experimentally on the basis of the coolant flow rate and temperature change through the calorimeter. The flow rate and temperature were measured by a precision turbine-type flowmeter and a thermopile device, respectively. To minimize conduction losses, the calorimeter is mounted away from the supporting structure by means of ceramic insulator-spacers (fig. 6). In addition, aluminized Kapton shields were positioned between the calorimeter and nearby colder components (liquid nitrogen lines, etc.) to minimize radiation losses. The positioning of some of these shields is also indicated in figure 6. In addition, the coolant fluid lines include ceramic tubular sections (not shown in fig. 6) to minimize calorimeter conduction losses along the lines.

MDC cooling. - As is indicated schematically in figure 5 and shown photographically in figure 7, a liquid-nitrogen-cooled copper jacket surrounds the MDC portion of the OST when the tube is positioned for testing in the TVTF. The MDC rejects heat by radiation to this jacket to simulate radiation to space in on-orbit operation. The interior surfaces of the jacket were uniformly coated with carbon in soot form; this soot was applied by a fuel-rich oxy-acetylene torch flame. A representative sample of this coated surface was shown to have a very high (exceeding 0.95) value of thermal emittance at low temperatures in spectrophotometer tests at the Lewis Research Center and therefore represents a good approximation of the absorptance of deep space. The jacket temperature is monitored by a thermocouple located near its top center.

Since the view of the MDC to space is partially blocked by nearby spacecraft components, a shadow shield to simulate that blockage (indicated schematically in fig. 5) was placed inside the cooled jacket, near the wall, in the appropriate orientation relative to the OST position. The shadow shield was patterned by radial projections through a cylindrical surface to the contours of the view-blocking components, assuming the MDC is a point heat source. The pattern on the cylindrical surface, the diameter of which matched that of the inside of the cooled jacket, was then fabricated of thin stainless-steel sheet. The surface of the pattern was estimated to approximate the optical properties of the blocking components acceptably. Finally, the shadow shield was properly positioned inside the cooled jacket, spaced about 0.00635 meter (0.25 in.) from the cooled wall. The MDC view to space blockage was calculated to be approximately 12 percent.

As will be detailed later in this report, the heat rejected from the MDC to the surrounding cooled jacket was determined on the basis of the MDC and jacket configurations, optical properties, and temperatures involved.

Output rf power measurement. - A water-cooled microwave rf load located outside the TVTF vacuum vessel was used to measure the rf output power of the OST. The load used is an impedance-matched device consisting of a section of waveguide terminated

with a low loss, thermally isolated glass tube in which the lossy dielectric distilled water is circulated. Since the water is the absorbing medium, the rf output power of the OST may be experimentally determined on the basis of the water flow rate and temperature change through the load. Stable load input water temperature and flow rates were regulated by means of a closed-loop heat exchanger and pump system located outside the vacuum vessel. A precision turbine-type flowmeter was used to measure the water flow rate, and a thermopile device was used to measure the water temperature change from load inlet to outlet.

Waveguide instrumentation. - The aluminum input and output OST waveguides, shown in figure 7, are relatively massive structures. Thin (0.000127 m (0.005 in.)) Kapton spacers were placed between a pair of connecting flanges on each of the waveguides to reduce the heat transfer away from the tube along these conduction paths. To determine the conduction heat-transfer rates along them, each waveguide was instrumented with a pair of thermocouples located 0.0127 m (0.5 in.) apart near the OST attachment flange. These instrument pairs are obscured by other components and are not visible in figure 7. The heat flow rates along the waveguides are determined on the basis of temperature gradients (assumed to be linear). These gradients are indicated by the thermocouple pairs, waveguide dimensions, and material thermal conductivity.

EXPERIMENTAL PROCEDURES

Calorimeter Calibrations

Both the OST baseplate calorimeter and the rf output load calorimeter systems were calibrated by substituting known heat loads for the calorimeters and then correlating these heat loads with the resulting coolant-temperature-change measurements at selected coolant flow rates and temperature levels. The known heat loads were supplied by a well-insulated resistance-heated tube system through which the coolant was passed. The heating element for this heat load (maximum capacity, 1 kW) was powered by a regulated dc power supply equipped with precision voltage and current measurement instruments. The calorimeter systems were calibrated over anticipated ranges of heat flow rates, coolant flow rates, and temperature levels. The calibration process was repeated at regular, frequent intervals during the testing to minimize potential errors which might be introduced due to changes in the characteristics of the flow system components.

OST Operation

After the OST was installed in the TVTF and the electrical, rf, and instrumentation

connections had been completed, the entire system was checked out. This was done by briefly (5 to 10 minute periods) operating the tube at saturated rf output power, ambient room conditions, and several baseplate temperatures. During this demonstration period, all systems were functional except for the liquid nitrogen supply to the radiation jacket surrounding the MDC portion of the OST. This system was not operated so that frost formation inside the TVTF could be avoided.

Following the ambient condition checkout, the TVTF vacuum vessel was closed and sealed. The surface electric heaters were then activated and the TVTF was heated to an average temperature of about 100° C. The temperature was held at that level for about 1 hour during the initial stage of the vacuum pumping of the vessel. Pumping continued until a pressure less than or equal to 1.33×10^{-6} newton per square meter (1×10^{-8} torr) was attained (as indicated by the vacion pump current requirement). The vessel pressure was held at this level for a minimum of 48 hours before OST vacuum-test operations were begun to avoid the possibility of localized regions of higher pressure within the TVTF. It should be noted that the input and output waveguides were vented to permit their evacuation to TVTF pressure. The maximum allowable pressure of the vacuum vessel during operation was 1.33×10^{-3} newton per square meter (1×10^{-5} torr). The maximum pressure observed during any of the tests, however, was no greater than 6.65×10^{-5} newton per square meter (5×10^{-7} torr); the average operating condition was about 6.65×10^{-6} newton per square meter (5×10^{-8} torr).

Vacuum operation of the OST began with establishing appropriate coolant flow rates through the baseplate and rf load calorimeters and liquid nitrogen flow in the MDC cooling jacket. The two OST vacion pumps (indicated in fig. 1) were then turned on. The cathode heater was first operated at 50 percent power for a minimum of 3 minutes before being adjusted to the 100 percent power condition. Following these events, the proper collector voltages were applied and the anode power was turned on. Finally, the beam was turned on when voltage was applied to the cathode. In order to avoid possible OST structural damage by overheating the coupled-cavity components, the maximum allowable operating level for body current was established at 10 milliamperes. This quantity was visually monitored continuously and a protective system was also used to interrupt tube operation if the body current exceeded the allowable limit. The procedure followed in turning the OST off was essentially the reverse of the sequence described for turning it on.

The rf operating conditions of the OST were established by the input rf driver frequency and power level. Since the OST baseplate temperature was determined by the calorimeter heating or cooling conditions (operator controlled), the OST could be operated over its entire rf operating range at baseplate temperatures ranging from -10° to 58° C.

Test Conditions and Sequences

The thermal-vacuum testing to which the OST's were subjected was designed to identify component heat-rejection rates and temperature levels, indicate possible failure modes, and, most desirably, provide assurances that the flight tube would perform satisfactorily throughout its mission in orbit by testing in a thermal environment equal to or more severe than the anticipated conditions. Specifically, the worst case operating flight predictions were the OST baseplate temperature extremes of 0° and 48° C. The more severe flight qualification temperature extremes included in the test procedure were -10° and 58° C. These test temperatures were jointly agreed to by NASA and the Canadian Department of Communications. A more detailed listing of OST baseplate thermal requirements is presented in reference 7. A further agreement was that the measured MDC cover temperature would not be permitted to fall below -85° C to assure structural integrity. The testing included operation at the CTS center band, lower band edge, and upper band edge frequencies (12.080, 12.038, and 12.123 GHz, respectively). The OST drive levels investigated were for the dc beam condition, the saturated rf output power condition, and the 6-decibel overdrive condition.

The specific thermal-vacuum test series performed on one OST, serial number 2025, is described in this report. The test series for this specific tube was selected because OST 2025 was used to type qualify the CTS flight OST (as described in ref. 7); in addition, it was designated as the flight backup unit. The thermal characteristics of OST 2025 are judged to be representative of those of the flight tube, although the flight unit has somewhat higher rf output power across the CTS operating band (ref. 7). The test series is presented in time-line form in figures 8(a) and (b). The figure details the test sequences for previbration and postvibration (qualification level) tests (ref. 7). Included in the test sequences are all anticipated OST rf operating conditions, a representative number (18) of temperature-reversal cycle tests, and power-off eclipse-simulating tests. The previbration test series required 37 hours and 24 minutes of OST operating time, of which 5 hours and 30 minutes were at the dc beam (zero rf output power) condition. The postvibration test series required 130 hours and 48 minutes of OST operating time, of which 48 hours and 7 minutes were at the dc beam condition. Results of the tests are described later in this report.

OST Thermal Equilibrium Criteria

The OST thermal test results presented herein were acquired at the thermal equilibrium condition, since this condition provides a relatively repeatable comparison point. Furthermore, without exception, the maximum or minimum component temperatures occur at the equilibrium condition. While temperature gradients and component

temperature rates of change maximize during the period prior to attaining thermal equilibrium, the rates of test condition change were regulated to a level judged to maintain the temperature gradients and rates of change at conservative, structurally safe levels. This was accomplished by limiting the rate of temperature change of the OST baseplate to a maximum of 1^{o} C per minute during test condition change periods. This rate of baseplate temperature change was estimated to approximate that which the OST would experience in its intended space application. Therefore, the characteristic time of system response to changes in the operating conditions will be representative of system operating conditions on the CTS spacecraft. An accurate determination of this thermal time characteristic of the OST is important for mission preeclipse operation planning to ensure that key OST temperatures remain in structurally safe ranges during eclipse periods. In the early phases of this testing program the time required for the OST to achieve essential thermal equilibrium following an operating condition change was approximately 2 hours. This time requirement is reflected in the testing sequence diagrams of figures 8(a) and (b).

OST thermal equilibrium requirements for a given test condition were considered to have been met when all the measured system temperatures remained stable (within 1^{o} C) for a minimum of 15 minutes. Furthermore, all flowmeters, calorimeter temperature differences, voltages, and power levels must have been stable (within 3 percent) for at least 15 minutes. In addition to these thermal requirements, an additional requirement that the OST body current remain stable (within 0.05 mA) for at least 15 minutes was observed.

Data Acquisition and Processing

The thermal, electrical, and rf characteristics of the OST were measured by an array of 96 instruments, the readings of which were recorded electronically on command. In addition, 35 of these measurements were displayed for continuous visual monitoring to assure proper facility operation. When a data set was taken, an analog scanner sampled the individual measurements five times over a period of approximately 0.25 second. The measurements were averaged, converted to floating point engineering parameters, and stored on magnetic tape by an interfacing digital computer. Finally, engineering calculations were performed by a digital computer, and data readouts were produced at the test site by a cathode ray tube - hard copy display unit.

Test Termination

After completing an OST thermal-vacuum test series, the tube was turned off and

the baseplate calorimeter and the MDC radiation jacket temperatures were returned to room ambient level (within 5^{o} C for not less than 15 min) before the support systems were turned off. The vacuum vessel was then backfilled (with nitrogen) to ambient pressure before opening for inspection.

CALCULATION PROCEDURES

OST Body Heat Rejection

The heat generated within the OST body which will be rejected to the CTS spacecraft thermal control system in orbit is measured in the TVTF by the baseplate calorimeter system. While the basic heat-rejection rate is readily determined as a function of coolant flow rate and temperature change through the calorimeter, as described in the APPARATUS AND EQUIPMENT section of this report, a correction to the basic measurement must be made to account for conduction along the aluminum input and output rf waveguides. This conduction correction was made on the basis of the temperature gradient indicated by the waveguide thermocouple pairs described earlier, along with the conduction path cross-sectional area and material thermal conductivity. Consequently, the heat-rejection rates of the OST body given in this report are the net rates calculated on this basis. Specifically, waveguide heat flow away from the OST body was added to the basic calorimeter measurement while heat flowing into the body was subtracted from the basic measurement. The net heat-rejection rate (in W) of the OST body will subsequently be indicated as Q_{bc}.

Unmeasured heat transfer between the OST body and the interior of the TVTF vacuum vessel includes that by radiation, by conduction between the baseplate calorimeter and its support structure, and by conduction along the electrical power and instrumentation wires. Baseplate thermal conduction isolation and radiation shielding was employed along with small-diameter instrumentation wires (see fig. 7) to minimize these effects. A worst-case estimate of less than 2-percent net body heat-rejection measurement error was made for these total effects. This amount of possible error was judged to be insignificant and was therefore not considered further.

MDC Heat Rejection

In the CTS spacecraft, the MDC portion of the OST protrudes from the spacecraft structure and is cooled by radiating directly to space. As indicated earlier, this configuration was simulated in the TVTF by surrounding the MDC with a liquid-nitrogen-cooled jacket equipped with a shadow shield to compensate for the MDC view to space

blockage which is present on the spacecraft. The MDC was inserted concentrically into the end of the jacket, which is approximately twice the largest diameter and three times the length of the MDC. The exterior surface of the MDC cover and the interior surface of the radiation jacket had thermal emittance values of 0.9 and 0.95, respectively.

To calculate the MDC heat-rejection rate, the relationship developed in reference 8 for gray isothermal concentric cylinders whose surfaces reflect diffusely was used. The equation was modified to accommodate partial view blockage and MDC cover nonuniform temperature distribution. Specifically, this modified relationship is

$$Q_{MDC} = \frac{A_{MDC}\sigma\left(T_{MDC}^4 - T_{jckt}^4\right)\eta}{\frac{1}{\epsilon_{MDC}} + \frac{A_{MDC}}{A_{jckt}}\left(\frac{1}{\epsilon_{jckt}} - 1\right)}$$

where

Q_{MDC}	heat-rejection rate of MDC cover, W
A_{MDC}	MDC cover external surface area, m^2
A_{jckt}	radiation jacket internal surface area, m^2
T_{MDC}	surface effective temperature (to be defined) of MDC cover, K
T_{jckt}	radiation jacket (near liquid nitrogen) temperature, K
ϵ_{MDC}	surface thermal emittance of MDC cover, 0.9
ϵ_{jckt}	radiation jacket interior surface thermal emittance, 0.95
σ	Stefan-Boltzmann radiation constant, $W/(m)^2(K)^4$
η	view blockage correction factor, 1 - blockage fraction, 0.88

The error due to determining the heat-rejection rate (relative to the space case) of the MDC cover by using the liquid-nitrogen temperature rather than the near-absolute-zero temperature of space in this relationship is insignificantly small.

Since A_{MDC} is very small relative to A_{jckt} and ϵ_{jckt} is nearly unity, the previous relationship reduces to

$$Q_{MDC} = A_{MDC}\epsilon_{MDC}\sigma\left(T_{MDC}^4 - T_{jckt}^4\right)\eta \tag{1}$$

where T_{MDC} is a weighted effective MDC cover surface temperature based on area zones whose temperatures are measured by one or more thermocouples. Specifically, in figure 4 the area represented by thermocouple TC1 is zone A_1; by thermocouples

TC2 and TC6 is zone A_2; by thermocouples TC3, TC4, TC7, and TC8 is zone A_3; and by thermocouple TC5 is zone A_4. The effective MDC surface temperature is defined as

$$T_{MDC} = \frac{A_1T_1 + 0.5\,A_2(T_2 + T_6) + 0.25\,A_3(T_3 + T_4 + T_7 + T_8) + A_4T_5}{A_{MDC}}$$

where

$$A_{MDC} = A_1 + A_2 + A_3 + A_4 \qquad m^2$$

and A_1, A_2, A_3, and A_4 are MDC cover area zones (m^2) and T_1 through T_8 are temperatures (K) indicated by thermocouples TC1 through TC8, respectively.

Using the calculation method described herein to determine Q_{MDC} provided satisfactory results. The accuracy of the calculations was readily evaluated at the dc beam (zero rf output power) OST operating condition. At this condition, the heat-rejection rate of the MDC cover is simply the difference between the total OST input electrical power (direct current and therefore able to be precisely measured) and the calorimetrically measured Q_{bc}. Furthermore, similar implicit determinations of the heat-rejection rates of the MDC cover were also routinely made at positive rf output power operating conditions. The rf output power was simultaneously measured calorimetrically (to be described) and thus provided the additional necessary component for energy balances at these conditions. Typically, the heat-rejection rate of the MDC cover calculated by using equation (1) agreed within 2 percent of the same quantity determined by the implicit energy-balance method.

The unmeasured heat transfer between the MDC cover and the interior of the TVTF vacuum vessel is essentially by conduction along the electrical and instrumentation wiring. A worst-case error estimate of less than 2 percent was made for this effect. Since this amount is considered insignificantly small, it was neglected in the calculation method employed.

Heat Transfer Between MDC and OST Body

The OST incorporates a thermal barrier system between the tube body and the MDC. This system, which was described earlier, consists of a copper radiation shield between the ground-potential MDC collector plate and support flange, a tortuous thermal path on the MDC cover external surface, and thin-wall tubular-stainless-steel collector-stack support posts (see fig. 2). A radially separated thermocouple pair was located on the

MDC high-voltage feedthrough flange inside the radius of the tubular-stainless-steel support post circle. Measurements made with this thermocouple pair provided an indication of the heat transfer between the MDC and the tube body at the instrumentation location. The heat transfer for this case was approximated from the Fourier conduction law applied to a long hollow cylinder with constant thermal conductivity. Specifically, this was

$$Q_F = \frac{2\pi kt(T_{F2} - T_{F1})}{\ln(r_{F2}/r_{F1})}$$

where

Q_F	heat-transfer rate from MDC to OST body, W
T_{F2}, T_{F1}	temperatures measured at thermocouple locations TF11 and TF12, respectively (see fig. 4), K
k	thermal conductivity of MDC flange material, W/(m)(K)
t	MDC flange thickness, m
r_{F2}, r_{F1}	radii on MDC flange to thermocouples TF11 and TF12, respectively (see fig. 4), m

While the radiation component of the heat transfer between the MDC and the OST body was not measured in this study, it was assumed to be negligibly small. This assumption was made because of the very low thermal emittance of the radiation shield material (copper) used in the MDC and the high effectiveness of even a single radiation shield.

OST rf Output Power

The rf output power of the OST is herein defined as the rf power at the coupled-cavity output port window. As described earlier, the rf power at a water-cooled termination load was measured calorimetrically. To refer the measured power to the OST window, the rf attenuation losses in the connecting waveguide sections must be included. To accomplish this, the output waveguide coupler (see fig. 1) and the waveguide section from the coupler to the load (see fig. 7) were separately calibrated and found to have insertion losses of 0. 15 and 0. 38 decibel, respectively. The calculation for OST rf output power then was

$$Q_{RF} = 10^{(L_C+L_G)/10} Q_{RF, L}$$

where

Q_{RF} OST rf output power, W

$Q_{RF, L}$ calorimetrically measured rf power at water-cooled load, W

L_C OST output waveguide coupler insertion loss, 0.15 dB

L_G coupler-to-load waveguide insertion loss, 0.38 dB

When the known values are substituted in the previous equation, it reduces to

$$Q_{RF} = 1.13\, Q_{RF, L}$$

The OST rf output power was also measured separately with an electronic power meter. The two measurements typically agreed within 2 percent.

Total OST Power Requirement

The total OST power requirement is readily determined from the measurements and measurement-based calculations described in the preceding sections. When making this calculation it must be noted that the rf attenuation (thermal) loss in the output waveguide coupler, because of its direct attachment to the OST body, is measured calorimetrically with the body heat-rejection rate. The OST power requirement is then expressed as

$$P_{OST} = Q_{bc} + Q_{MDC} + Q_{RF, C}$$

where

P_{OST} total OST power requirement, W

$Q_{RF, C}$ rf power at entrance to coupler-to-load waveguide section, W

Substituting the known value for L_G in

$$Q_{RF, C} = 10^{L_G/10} Q_{RF, L}$$

gives

$$Q_{RF,\,C} = 1.09\, Q_{RF,\,L}$$

This thermal-measurement-based total OST power requirement was directly compared with the measured electrical power requirement; it typically agreed within 5 percent. The electrical power requirement was determined by summing the collector power, the anode power, the cathode heater power, and the power loss due to electron beam interception.

Experimental Error Assessment

Throughout this report an effort has been made to inform the reader as to the estimated worst-case effects which unmeasured heat transfer would have on measured or measurement-based calculations of heat-transfer rates. Also, results of comparisons between quantities that were measured independently have been routinely reported. The purpose of these estimates and comparisons is to indicate the level of confidence which can be placed in the experimental results presented in this report. Another important indication relevant to this confidence level is the accuracy of the instruments used to make the requirement measurements.

An assessment of the experimental error based on the advertised specifications of the instruments used in this study, within the typical ranges of their use, was performed. Included in the analysis were thermocouples, flowmeters, differential temperature measurement devices (thermopiles), operational amplifiers, voltmeters, ammeters, signal converters, and the data acquisition system. The assessment indicated that the root mean square (rms) error was within ±4 percent when determining the heat-rejection rate and rf output power of the OST body. On a similar basis, the measured temperature rms error was determined to be about ±2 percent.

A separate error analysis was performed for the instruments used to make the electrical power measurements that were used for comparison with the thermal measurements of this study. This analysis indicated the OST rf output power, measured by means of a rotary-vane attenuator and power meter, had a rms error within ±7 percent, while the electrical power measurements had a rms error of about ±4 percent.

RESULTS AND DISCUSSION

It was noted in the APPARATUS AND EQUIPMENT section that a number of OST's had been tested during this investigation in a manner similar to that described in this report. Each OST, having somewhat different characteristics, yielded experimental results which also were individually different. The experimental results emphasized in

this report are those developed from the specific test sequences performed with OST 2025, and they are considered to be representative of the OST in operation onboard CTS. Reference 7 indicates OST 2025 is identical in configuration to the flight OST and was similarly trim focused during processing at the elevated temperature. The OST onboard the spacecraft was flight qualified by similarity with OST 2025, which was designated as the flight backup unit.

The test series for OST 2025, detailed in figure 8, was done in two steps, one before and one after the OST was vibration tested. The vibration-testing program is described in reference 7. In view of this, much of the experimental information presented herein will be identified as either previbration or postvibration testing results. The test results identified as 1(a), 1(b), and 1(c) in figure 8 will not be presented, since they were non-thermal-equilibrium checkout tests performed at ambient room conditions.

Table II presents the major operating thermal characteristics of OST 2025 which resulted from the previbration and postvibration test sequences. The results presented are not average or mean values for several "identical" test conditions, but they are specific values for one particular test that was judged to be typical of the test condition stated. Nominally identical operating conditions were repeated where indicated in figure 8, but the extreme difficulty in exactly duplication the operating conditions led to small variations in the test results. A discussion of these variations is presented later. Results of test 6 (fig. 8), the simulated extended eclipse cold-soak tests, will be described separately.

OST Body Heat Rejection

Table II shows that the heat-rejection rate of the OST body ranged from 7.6 watts at the dc beam (zero rf output power) condition to 184.5 watts at the center-band (12.080 GHz) frequency for the 6-decibel overdrive condition; the OST baseplate temperature was at 45° C for both cases. The maximum heat-rejection rate measured with the OST at saturated rf output power at the center-band frequency with a baseplate temperature of 45° C (normal anticipated operating point in space operation) was 146.8 watts. These tests required about 2 hours of stable operation after a change in operating conditions to achieve OST thermal equilibrium. Because of the nature of the heat generation within the OST body (circuit losses), the companion parameter to the heat-rejection rate is the body current level. The body current is in turn influenced directly as the OST drive level and the baseplate temperature. The body current levels for the dc beam, overdrive, and saturated rf output power conditions mentioned previously were 1.83, 8.94, and 4.08 milliamperes, respectively. The influence of baseplate temperature is evidenced from the results shown in table II, where the body current levels at OST

saturated rf output power are 3.32, 4.08, 4.20, 4.51, and 4.57 milliamperes at baseplate temperatures of 25°, 45°, 48°, 53°, and 58° C, respectively.

Variations in the OST baseplate heat-rejection rates, body current levels, and other thermal parameters for the 16 successive nominally duplicate temperature-reversal test cycles performed in the postvibration test sequence are shown in figures 9 and 10. In these tests, the OST operating conditions were alternately established at saturated rf output power at the center-band frequency with a baseplate temperature of 48° C and at dc beam condition with a baseplate temperature of 0° C (tests 7 and 8, respectively, as shown in fig. 8). With the exception of a single interruption for another type of test, the cyclic tests were performed consecutively. Figure 9 displays the cycle to cycle variations in the OST total power requirement, rf output power, MDC and body heat-rejection rates, and body current for the saturated rf output power at the center-band frequency condition at a 48° C baseplate temperature. Similarly, cycle to cycle variations in power requirement, MDC and body heat-rejection rates, and body current for the dc beam condition at a 0° C baseplate temperature are shown in figure 10. It is noted that the percentage variations of body heat-rejection rate and body current of figure 10, the dc beam values, are greater than those of figure 9, the saturated rf output values. This is due to the difficulty of exactly duplicating the operating conditions at low baseplate temperatures. The corresponding cycle to cycle equilibrium baseplate temperature variations for these tests were about ±3° C.

Various temperatures measured on the body structure of OST 2025 are listed in table III. While the temperature distribution is different for each of the operating conditions listed, it should be noted that for the saturated rf output condition shown the maximum temperature measured was on the output pole piece of the coupled-cavity section (thermocouple TOUTP). Other nearby thermocouples measured slightly lower temperatures. As would be expected, all the body temperatures are lower for the dc beam cases than they are for those with rf output power.

The temperatures measured by the four thermistors are not used for any calculations in this study, but they are listed in table III. Because only thermistor data will be relayed from the OST while in orbit, these data are included here for reading comparison with nearby thermocouples for possible assistance in flight data interpretation.

An examination of the values presented in table II, figures 9 and 10, and all other OST 2025 test data indicates no statistically significant evidence of changes in the baseplate heat-rejection rate or body current level that can be attributed to either the OST vibration testing or the temperature-reversal cycle testing sequence.

MDC Heat Rejection

The MDC heat-rejection rate ranged from 141.9 watts with the OST at saturated rf

output power at the center-band frequency and 25° C baseplate temperature to 192.3 watts at the dc beam condition and 45° C baseplate temperature. At the normal anticipated operating condition (saturated rf output power at center-band frequency and 45° C baseplate temperature) the maximum heat-rejection rate was 147.0 watts. These values appear in table II. While the baseplate temperatures are indicated here to assist in identifying the specific data in the table, the MDC heat-rejection rates appear to be insensitive to the OST baseplate temperature level. Values of the weighted effective MDC cover temperature T_{MDC} also appear in this table along with the maximum temperature measured. The maximum MDC cover temperature shown (in table II) is 216.7° C at the location of thermocouple TC7 (refer to fig. 4) during a test with the OST at the dc beam condition and 45° C baseplate temperature. During another test at the same operating conditions, the maximum temperature noted (at the same location) was 227° C. Thermocouple TC7, which is positioned on the MDC cover 0.09 meter (3.6 in.) from the high-voltage feedthrough flange surface, is approximately at the location of the outer edge of MDC plate 8 (see figs. 2 and 4). For all the test conditions studied, except for the dc beam conditions, the maximum MDC cover temperatures were measured at the axial positions of thermocouples TC2 and TC6. These instruments, which are positioned on the MDC cover 0.0635 meter (2.5 in.) from the high-voltage feedthrough flange surface, are approximately at the location of the outer edge of MDC plate 5. For all the dc beam condition tests, the maximum MDC cover temperatures were measured at the axial positions of thermocouples TC3 and TC7. Temperatures measured on OST 2025 (and several other OST's) on the MDC cover at points 180° apart at the same axial position for a given test condition agreed well (within 9° C maximum, with most differences of the order of 2° to 5° C). This suggests relatively uniform circumferential internal heating. The MDC cover instrumentation was not adequate to assess the effects on cover temperatures at those locations where internal shadowing occurs because of the ceramic MDC plate stack support posts.

As with the OST body, the MDC required about 2 hours of stable operation to achieve thermal equilibrium after a change in operating conditions.

Figures 9 and 10 display the postvibration-testing cycle to cycle variations in the MDC heat rejection for the saturated rf output power and dc beam conditions at baseplate temperatures of 48° and 0° C, respectively. The relatively small, random variations in this parameter indicate the temperature-reversal cycle testing had no measurable effect. Furthermore, the information presented in table II indicates no change in MDC thermal characteristics that can be attributed to the vibration-testing procedure.

Heat Transfer Between MDC and OST Body

Characteristically, the direction of heat transfer across the conduction barrier (or

thermal choke) between the MDC and the OST body was toward the MDC for the saturated rf output power tests and toward the body for the dc beam tests. Typical values of these heat-transfer rates are listed in table II. While an observer might first assume that heat transfer would always be toward the OST body because of the much higher general MDC temperature, this is not the case. An examination of the relative temperature levels of thermocouples TOUTP (or TSWST) and TFLING in table III provides an indication of the temperature differences in the near vicinity of the thermal choke. These temperature differences determine the heat-transfer direction but not the magnitude. For the saturated rf output power tests, the temperatures indicated by TOUTP (and TSWST) are invariably greater than those indicated by TFLING; for the dc beam tests, the reverse is always the case. While table III contains only a very small sampling of the experimental results obtained during the course of the study reported herein, the results not included also support these findings. Since the measured heat-transfer rates are quite low, about 2 watts maximum, the effectiveness of the CTS OST thermal choke configuration must be considered to be satisfactory.

While OST 2025, which provided the MDC to OST body heat-transfer results of table III, was fitted with only one pair of gradient-indicating thermocouples, redundant instrument pairs on other OST's indicated essentially circumferentially uniform heat transfer across the thermal choke for these instrumented locations.

OST rf Output Power

The rf output power characteristics of OST 2025, shown by comparing the values listed in table II, were unaffected by the vibration-testing procedure within the range of probable experimental error. The power at saturation (center-band frequency) was about 169 watts; it appeared to remain constant over the range of baseplate temperatures examined. Power reductions relative to saturated rf output power at center-band frequency were experienced at saturated power at the upper and lower band edge frequencies for the same baseplate temperature. The 6-decibel overdrive condition at the center-band frequency resulted in a reduction in rf output power of about 80 percent relative to saturated power at the same frequency and baseplate temperature.

Figure 9 shows the cycle to cycle variations in rf output power during the postvibration temperature-reversal cycle tests. Again, taking into account the measurement error probability and the difficulty involved in exactly duplicating test conditions, it must be assumed that no measurable changes in the rf output power level occurred as a result of the temperature-reversal cycle testing.

Simulated Extended Eclipse Test

The CTS spacecraft experiences twice-annual Earth eclipse seasons of about 48 days each. During these seasons, the spacecraft is in the Earth's shadow one time each day for a maximum of about 72 minutes. During the time in the Earth's shadow (in addition to programmed periods) the OST is placed in a standby status with all power off except for the 50-percent cathode heater power. During this standby status period, the MDC continues to radiate thermally to space with an accompanying, initially rapid, surface temperature reduction. The OST body temperature reduces at a lower rate during this period. Since the MDC cover uses a large number of ceramic to metal attachments, at some critical temperature the dimension differences caused by differences in thermal contraction rates could cause distortions and/or separations which could result in tube damage and malfunction. To ensure that the critical low temperature is not reached during a nonoperating eclipse period, and to determine the general MDC cooldown characteristics, a simulated extended eclipse test (test 6, fig. 8) was devised and performed.

The eclipse test began by turning off all OST power except for keeping the cathode heater power at 50 percent. The OST baseplate temperature was reduced to near -10° C over a period of about 2 hours and held at that general level. This baseplate temperature was selected since it was specified (ref. 7) as the OST minimum turn-on temperature for component qualification. The MDC and baseplate temperatures were monitored for about 6 hours, after which the OST was returned to operation at the saturated rf output power level at centerband frequency. The baseplate temperature, area-averaged MDC temperature, and MDC minimum temperature profiles with time during the post-vibration test are shown in figure 11. At 72 minutes into the test, which corresponds to approximately the maximum Earth eclipse period that the CTS spacecraft will encounter, the minimum MDC cover temperature (about 8° C) was found to be on the end dome. At the end of the eclipse period (6 hr and 7 min) this lowest temperature had reduced to -67.5° C, well above the minimum allowable temperature of -85° C described earlier. The heat transfer between the MDC and the OST body varied from 0.03 watt (to the OST body) at the beginning of the test to 1.0 watt (to the MDC) at about 72 minutes to 0.36 watt (to the MDC) at the end of the test. At the end of the eclipse test period, the OST was turned on and adjusted to the saturated rf output power condition at center-band frequency. No difficulty was encountered in reaching this condition.

OST Thermal Interface Conditions

Qualitative assessments of the general condition and effectiveness of the several OST thermal interfaces can readily be made from the temperature data acquired during

this investigation. Specifically, the temperature drop across the forward (closest to the MDC) body to mounting saddle interface is indicated by the difference in the readings of thermocouples TBAR3 and TSDL1 (refer to fig. 4), while the rear body to saddle interface temperature difference is indicated by the difference in the readings of TBAR1 and TSDL2. Similarly, the forward and rear saddle to baseplate temperature differences are indicated by the differences between the readings of TSDL1 and TTBP1 and TSDL2 and TTBP2, respectively. Finally, the forward and rear baseplate to calorimeter temperature differences are indicated by the differences in the readings of TTBP1 and TBC4 and TTBP2 and TBC2, respectively. The relatively low temperature difference levels indicated by the values shown in table III were found to be typical of the several OST's tested and were generally consistent for similar operating conditions during the test series, indicating satisfactory and well-secured interfaces. Significant increases or changes in these temperature differences could be indicative of improperly fitted or loose thermal interfaces.

SUMMARY OF RESULTS

Several 12-gigahertz, 200-watt (nominal) rf amplifier output stage tubes (OST's) developed for use in the Communications Technology Satellite were tested in a simulated space environment to determine their equilibrium thermal characteristics. This information was required for the design of the spacecraft thermal control surfaces and the variable conductance heat pipe system. The testing procedure was designed to separately identify the heat-rejection rates of the OST body (rf interaction, coupled-cavity, slow-wave structure section) and the multistage depressed collector (MDC) portions of the tube for a range of operating conditions. These heat-rejection rates are not currently calculable with acceptable accuracy by analytical means. Particular emphasis was placed on the characteristics of the flight backup and flight-qualification tube (OST 2025), which is identical in configuration to and assumed to be representative of the flight tube. OST 2025 was subjected to a testing sequence that included operation over the entire anticipated operating drive range from the dc beam (zero rf output power) to the 6-decibel overdrive condition. The tube baseplate temperature was varied from -10° to 58° C with testing emphasis on the normal anticipated operating temperature (45° C). The test sequence included evaluation periods before and after OST flight-qualification vibration testing, extensive temperature-reversal cycle testing, and simulated extended spacecraft-in-eclipse conditions. The results of this experimental study, along with some general observations, are summarized in the following statements:

1. The experimental and calculation procedures used in this investigation were satisfactory for the purpose intended. The test results were repeatable, reasonable, and internally consistent. While the experimentally determined individual OST body and

MDC heat-rejection rates could not be compared directly with values of these quantities determined independently, the net system heat-rejection rates agree quite well (within about 2 percent, generally) with the net OST electrical power requirement measurements for the various operating conditions investigated.

2. The OST body and MDC require a period of stable operating conditions of about 2 hours following a change in conditions to achieve thermal equilibrium.

3. The testing procedures revealed no statistically significant evidence of changes in the OST thermal characteristics or rf output power which can be attributed either to the vibration testing or the temperature-reversal cycle testing sequence.

4. Measured values of the heat-rejection rate of the OST baseplate for OST 2025 ranged from 7.6 watts at the dc beam (zero rf output power) condition to 184.5 watts at the 6-decibel overdrive condition at center-band frequency (12.080 GHz) with the baseplate temperature at 45° C for both cases. The maximum heat-rejection rate measured with the OST at normal anticipated operating conditions in space (saturated rf output power, center-band frequency, baseplate temperature 45° C) was 146.8 watts. The OST body current level, which was observed to vary directly with drive level and baseplate temperature, ranged from 1.70 to 9.08 milliamperes.

5. The maximum OST body temperature measured was on the output pole piece of the coupled-cavity section. While this temperature varied directly as the OST drive level and baseplate temperature, it was about 83.7° C at the normal anticipated space operating conditions (see item 4).

6. The MDC heat-rejection rates ranged from 141.9 watts with the OST in the saturated-rf-output-power condition at center-band frequency to 192.3 watts at the dc beam condition. At the normal anticipated space operating conditions, the maximum measured heat-rejection rate was 147.0 watts. These heat-rejection rates appear to be insensitive to OST baseplate temperature, only moderately sensitive to operating frequency, and primarily an inverse function of rf output power.

7. The maximum MDC cover temperature measured on each of the OST's tested in this program occurred while operating at the dc beam condition. These temperatures occurred at a different location (further from the OST body) than the maximum MDC cover temperatures for tests at saturated rf output power conditions. The maximum MDC cover temperature measured on OST 2025 was 227° C.

8. Temperatures measured on the MDC cover at points 180° apart at the same axial position for a given test condition agreed well (within 9° C maximum, with most differences of the order of 2° to 5° C) for OST 2025 and other OST's. This suggests relatively uniform circumferential internal heating. The MDC cover instrumentation was not adequate to assess the effects on temperatures at those cover locations where internal "shadowing" occurs because of the ceramic MDC plate stack support posts.

9. The direction of heat transfer across the conduction barrier, or thermal choke, between the MDC and the OST body was toward the MDC in the saturated rf output power

tests and toward the OST body for the dc beam tests. The measured heat-transfer rates ranged, depending on the operating conditions, from 0.56 (body to MDC) to 2.09 watts (MDC to body) with 1.77 watts (body to MDC) a typical value for the normal anticipated space operating conditions. These relatively low heat-transfer rates indicate the CTS OST thermal choke configuration is effective. Measurements made with those OST's which had redundant, circumferentially distributed thermal choke instrumentation indicated relatively uniform heat-transfer rates at the locations instrumented.

10. Saturated OST rf output power appears to be insensitive to baseplate temperature level within the range of test conditions investigated.

11. Results of the tests which simulated an extended spacecraft-in-eclipse condition indicate the MDC cover dome (end cap) reached the lowest measured temperature (8° C) on the OST at the end of 72 minutes, the time corresponding to the maximum period of shadow in an Earth eclipse. At the conclusion of the tests (6 hr and 7 min), the minimum OST temperature (-67.5° C) occurred at the same point on the MDC. At the end of these tests the OST was turned on and adjusted to the saturated-rf-output-power, center-band frequency condition without difficulty.

12. The thermal bonds between the OST body and aluminum saddles, between the saddles and aluminum baseplate, and between the baseplate and aluminum calorimeter appear to be of satisfactory constant quality. This assessment is based on an examination of the temperature drops across these interfaces relative to the OST body heat-rejection rates to the calorimeter.

Lewis Research Center,
National Aeronautics and Space Administration,
Cleveland, Ohio, May 31, 1978,
610-22.

REFERENCES

1. Donoughe, Patrick L.; and Hunczak, Henry R.: CTS (Hermes) - United States Experiments and Operations Summary. NASA TM-73830, 1977.

2. Alexovich, R.: The 200 Watt SHF Transmitter Experiment Package. NASA TM X-68106, 1972.

3. Franklin, C. A.; and Davison, E. H.: A High-Powered Communication Technology Satellite for the 12 and 14 GHz Bands. AIAA Paper 72-580, Apr. 1972.

4. Kosmahl, Henry G.; McNary, B. D.; and Sauseng, Otto: High Efficiency, 200 Watt, 12-Gigahertz Traveling Wave Tube. NASA TN D-7709, 1974.

5. Kosmahl, Henry G.: A Novel, Axisymmetric, Electrostatic Collector for Linear Beam Microwave Tubes. NASA TN D-6093, 1971.

6. Kavanagh, Francis E.; Alexovich, Robert E.; and Chomos, Gerald J.: Evaluation of Novel Depressed Collector for Linear-Beam Microwave Tubes. NASA TM X-2322, 1971.

7. Chomos, Gerald J.; and Curren, Arthur N.: Description and Expected Performance of Flight-Model, 12-Gigahertz, Output Stage Tube for the Communications Technology Satellite. NASA TM X-3441, 1976.

8. Eckert, Ernest R. G.; and Drake, Robert M., Jr.: Analysis of Heat and Mass Transfer. McGraw-Hill Book Company, Inc., 1972, p. 633.

TABLE I. - CTS OST 2025 THERMAL

INSTRUMENTATION IDENTIFICATION

Instrument notation[a]	Location
Thermocouples:	
TBC2, TBC4	OST baseplate calorimeter surface
TC1 to TC8	MDC cover
TFLNG	MDC support flange
TF11	MDC support flange at radius r_1
TF12	MDC support flange at radius r_2
TRFCM	Refocusing magnet top surface
TOUTP	Output pole piece top surface
TSWST	Fourth-from-last pole piece top surface
TMAG1	Twelfth-from-last pole piece top surface
TMAG2	Second sever top surface
TBAR1 to TBAR3	Thermal bus bar opposite waveguide side
TBAR4	Thermal bus bar at output waveguide
TCC1	Input waveguide transformer top surface
TCC2	Output waveguide transformer top surface
TSDL1	Body saddle block at output end
TSDL2	Body saddle block at input end
TTBP1	Baseplate near output end
TTBP2	Baseplate near input end
TJCKT	Liquid-nitrogen-cooled MDC jacket top
Thermistors:	
T1MDC	MDC cover
T2MDC	MDC support flange
TBODY	Thermal bus bar at output waveguide
TOC	Output waveguide coupler

[a]See diagram in fig. 4.

TABLE II. - CTS OST 2025 THERMAL CHARACTERISTICS SUMMARY

Output rf power, Q_{RF}, W	Operating frequency,[a] GHz	OST baseplate			MDC cover			MDC to OST body heat-transfer rate, Q_F, W	Total OST power, P_{OST}, W
		Nominal temperature,[b] °C	Heat-rejection rate, Q_{bc}, W	Body current, mA	Mean effective temperature, °C	Maximum measured temperature, °C	Heat-rejection rate, Q_{MDC}, W		
Previbration test series									
[c]170.9	12.080	25	144.2	3.36	139.4	174.7	141.9	-----	451.2
[d]0	------	45	12.8	1.98	171.9	216.7	192.3	-----	204.9
[c]169.1	12.080	↓	136.8	3.86	143.0	178.8	147.0	-----	446.7
[e]33.9	12.080		173.7	9.08	153.2	192.6	161.9	-----	368.4
[c]152.0	12.123		122.1	3.78	143.8	181.8	148.1	-----	417.0
[c]162.4	12.038		137.8	3.92	152.6	188.8	160.9	-----	455.7
[c]169.9	12.080	53	140.9	4.21	141.6	178.9	144.9	-----	450.0
[c]169.7	12.080	58	132.7	4.27	142.9	179.0	146.9	-----	443.5
Postvibration test series									
[c]167.8	12.080	25	136.1	3.32	143.0	180.4	146.9	-0.56	445.2
[d]0	------	45	7.6	1.83	171.9	214.8	192.2	.76	201.1
[c]168.9	12.080	↓	146.8	4.08	140.7	178.1	143.7	-1.77	453.6
[e]37.5	12.080		184.5	8.94	149.2	187.6	155.9	-1.69	376.5
[c]150.1	12.123		132.0	4.06	141.7	179.3	145.1	-1.57	422.1
[c]160.2	12.038		130.1	3.93	148.0	185.3	154.1	-1.61	438.9
[c]168.9	12.080	53	140.3	4.51	139.9	176.1	142.6	-1.89	446.0
[c]166.4	12.080	58	129.7	4.57	141.8	178.8	145.2	-----	435.7
[c]168.4	12.080	48	138.6	4.20	140.4	177.1	143.2	-1.49	444.4
[d]0	------	0	20.2	1.70	167.0	210.8	184.0	2.09	204.9

[a]Frequency: center band, 12.080 GHz; upper band edge, 12.123 GHz; lower band edge, 12.038 GHz.

[b]Maximum measured baseplate temperature.

[c]Saturated rf output power condition.

[d]Zero rf output power (dc beam) condition.

[e]6-Decibel overdrive condition.

TABLE III. - CTS OST 2025 MEASURED TEMPERATURES AT SELECTED EQUILIBRIUM CONDITIONS

Instrument[a]	Output rf power, W			
	0 (dc beam)	168.9 (Sat.)	168.9 (Sat.)	0 (dc beam)
	Operating frequency, GHz			
	N.A.[b]	12.080	12.080	N.A.[b]
	Nominal baseplate temperature, °C			
	45	45	53	0
	Temperature, °C			
TBC2	44.8	38.6	46.0	-2.7
TBC4	44.6	44.6	52.2	.2
TC1	112.7	100.2	100.9	106.3
TC2	204.2	174.0	173.4	197.8
TC3	207.2	163.3	162.7	202.7
TC4	193.4	149.4	148.6	190.1
TC5	134.3	95.7	94.6	132.5
TC6	211.0	178.1	176.1	205.8
TC7	214.8	165.7	163.8	210.8
TC8	197.3	148.2	146.6	194.3
TFLNG	55.2	62.2	68.6	16.2
TRFCM	49.9	80.0	87.8	8.3
TOUTP	49.1	83.7	92.3	5.4
TSWST	48.3	83.1	91.7	4.6
TMAG1	49.5	77.5	86.3	4.3
TMAG2	51.5	68.5	77.4	6.9
TBAR1	51.5	58.5	67.9	6.5
TBAR2	46.9	62.0	72.7	5.3
TBAR3	47.8	63.9	72.8	-----
TBAR4	46.9	58.3	66.7	3.7
TCC1	49.1	61.4	70.1	9.1
TCC2	47.5	88.3	96.3	5.4
TSDL1	46.9	55.7	63.8	-----
TSDL2	47.6	49.1	56.9	3.4
TTBP1	45.8	47.2	54.9	-----
TTBP2	44.9	39.5	46.7	-----
TJCKT	-191.9	-191.9	-190.8	-193.6
T1MDC	175.7	157.1	152.6	174.1
T2MDC	46.9	53.1	58.2	15.2
TBODY	47.3	59.2	66.9	5.1
TOC	38.4	69.6	73.6	13.1

[a]Refer to table I for instrument locations.

[b]Not applicable.

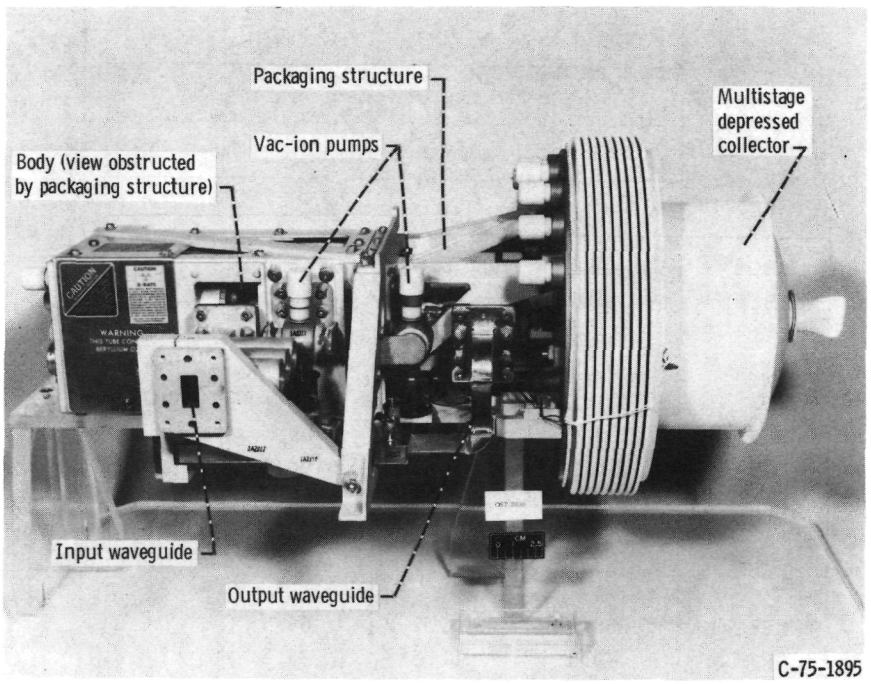

Figure 1. - Output stage tube for the Communications Technology Satellite.

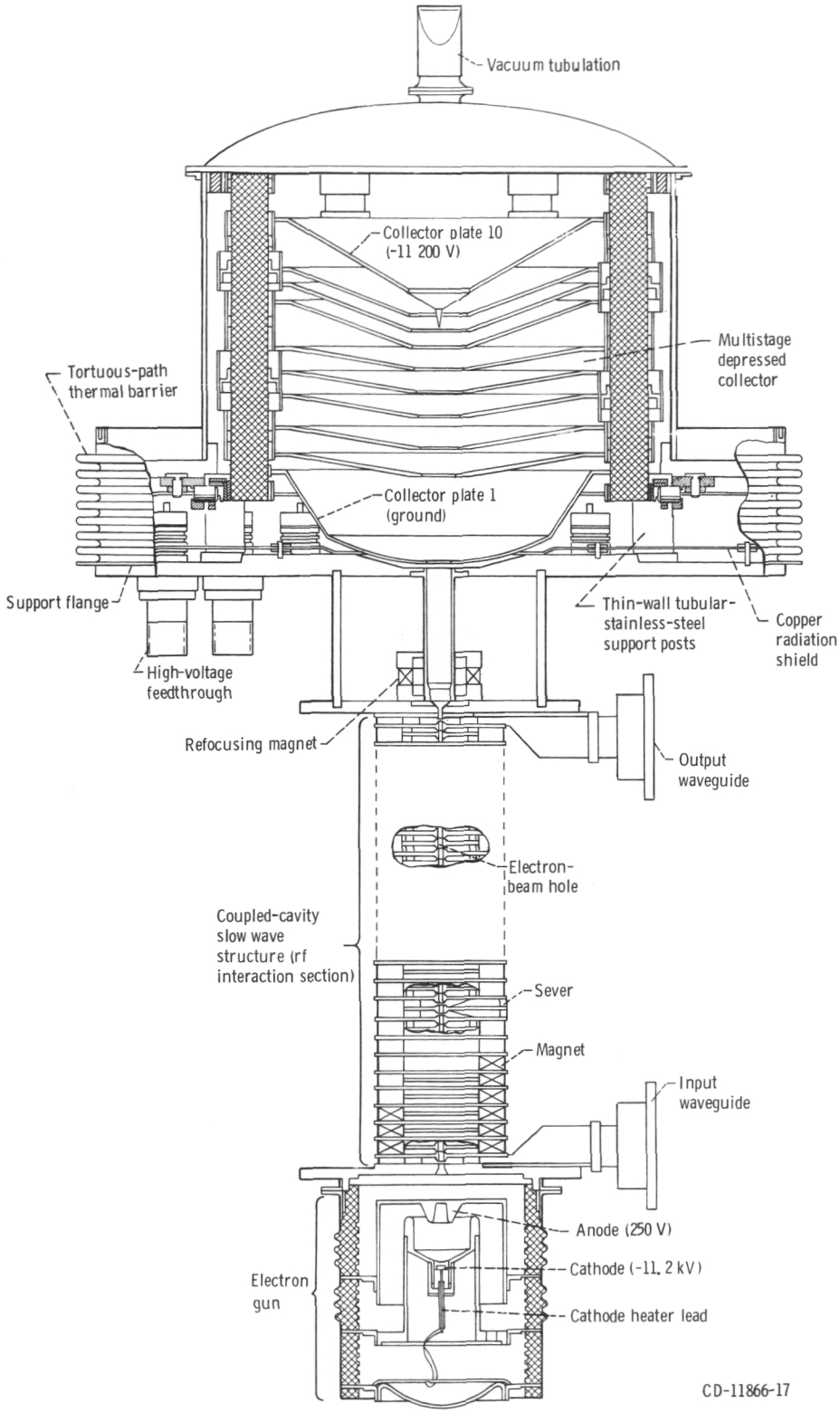

Figure 2. - Coupled-cavity traveling wave tube with multistage depressed collector.

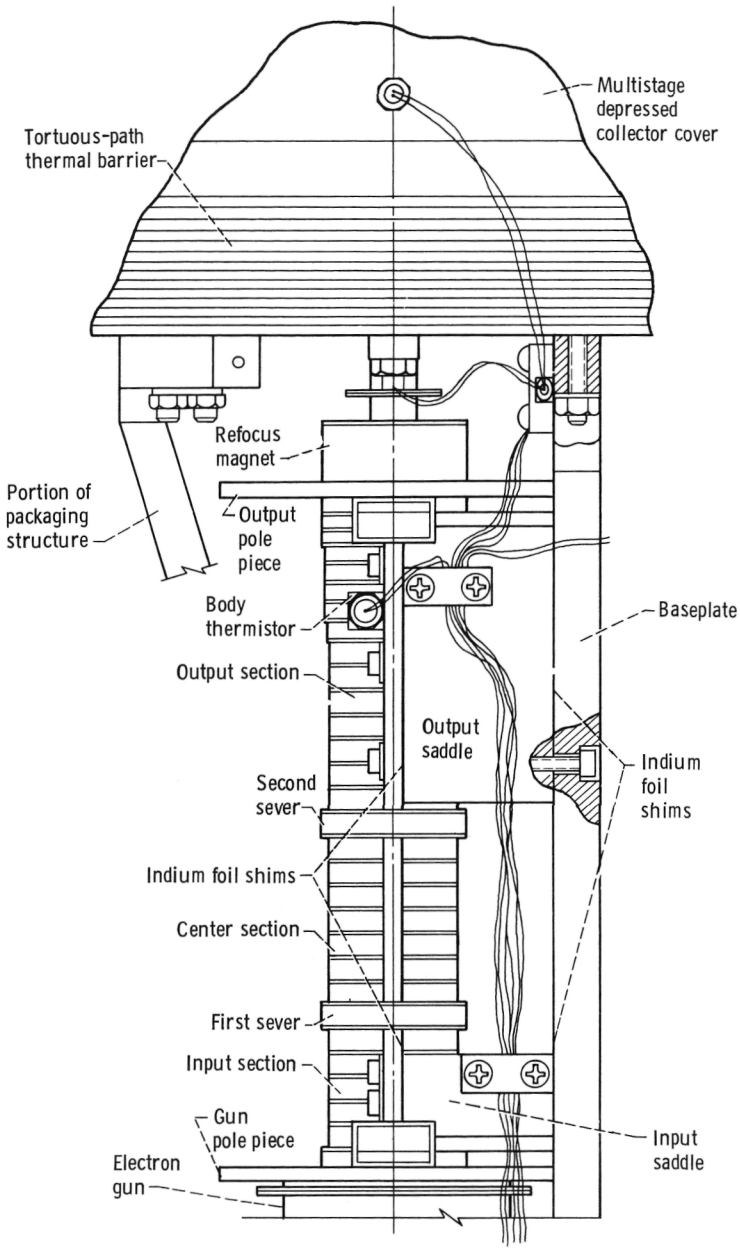

Figure 3. - Detailed view of coupled-cavity traveling-wave-tube body.

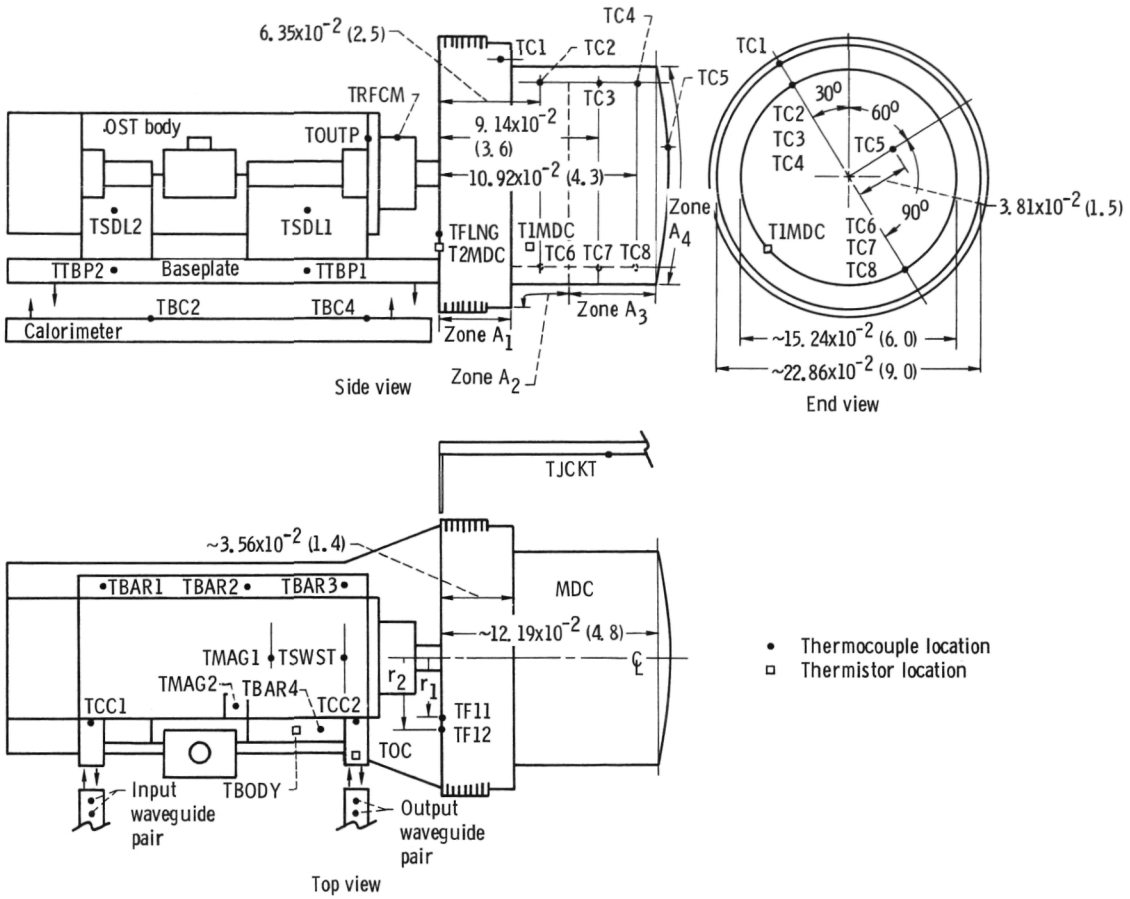

Figure 4. - Schematic of thermal instrumentation (see table I) on CTS OST 2025. All dimensions in meters (in.).

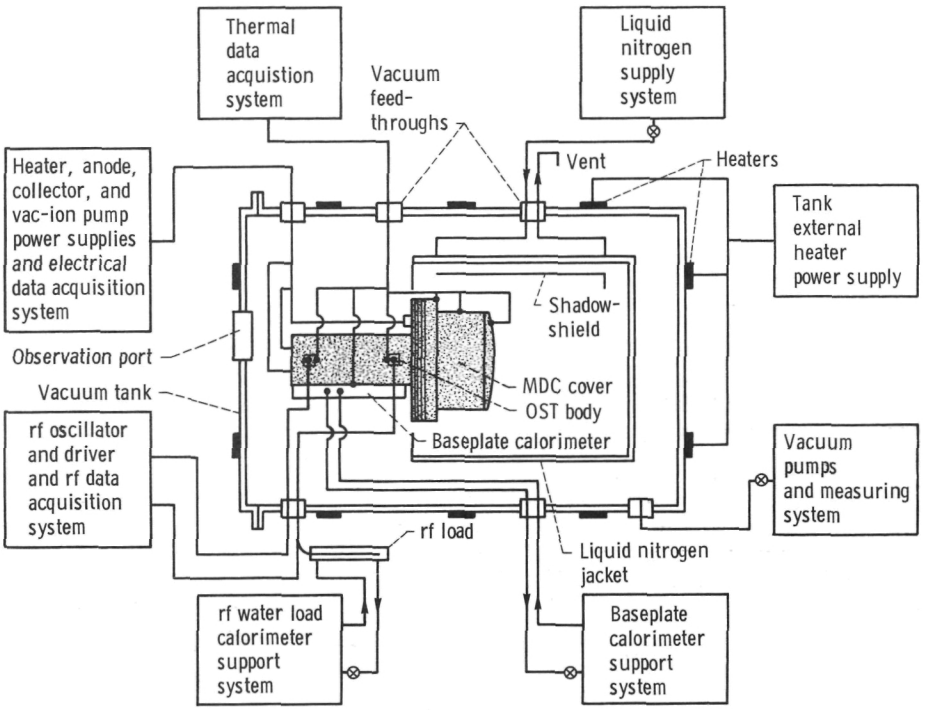

Figure 5. - Schematic of CTS OST thermal-vacuum test facility.

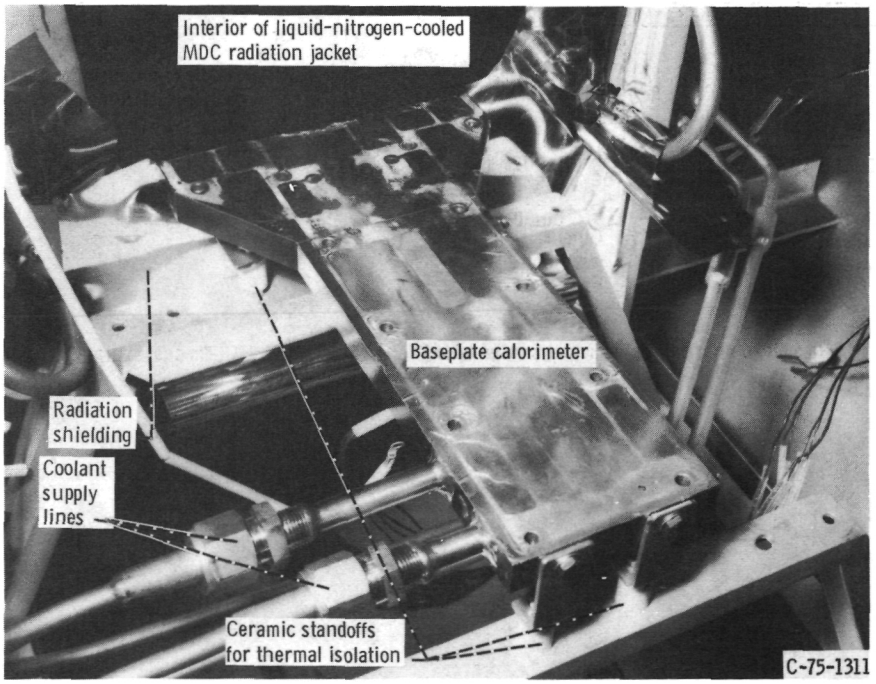

Figure 6. - CTS OST baseplate calorimeter mounted inside TVTF vacuum vessel.

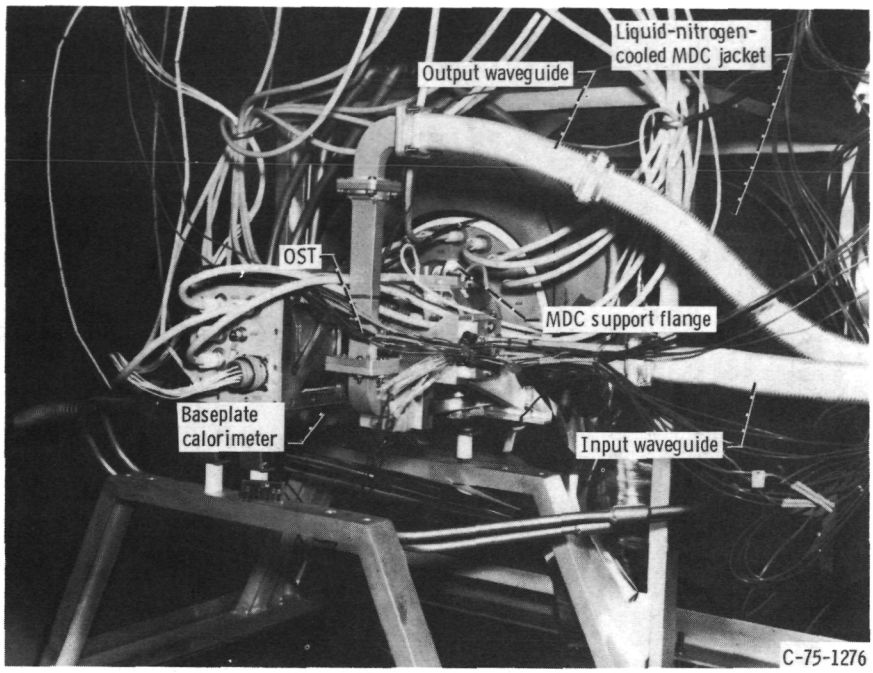

Figure 7. - View of CTS OST mounted in TVTF showing liquid-nitrogen-cooled MDC space-simulating jacket.

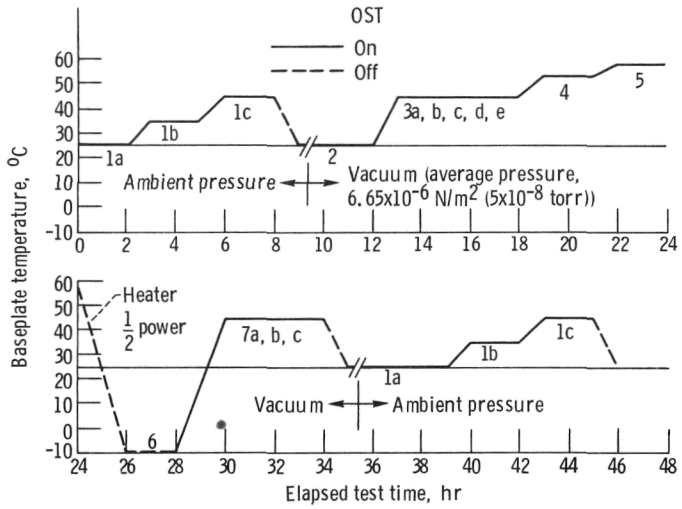

Test and step	OST baseplate temperature, °C	OST operating frequency, GHz	OST drive level
1a	25	12.080	Saturation
b	35		
c	45		
2	25		
3a	45		Zero (dc beam)
b			Saturation
c			6-dB overdrive
d		12.123	Saturation
e		12.038	
4	53	12.080	
5	58		
6	-10		Off (heater ½ power)
7a	45		Zero (dc beam)
b	45		Saturation
c	45		6-dB overdrive

(a) Previbration test sequence.

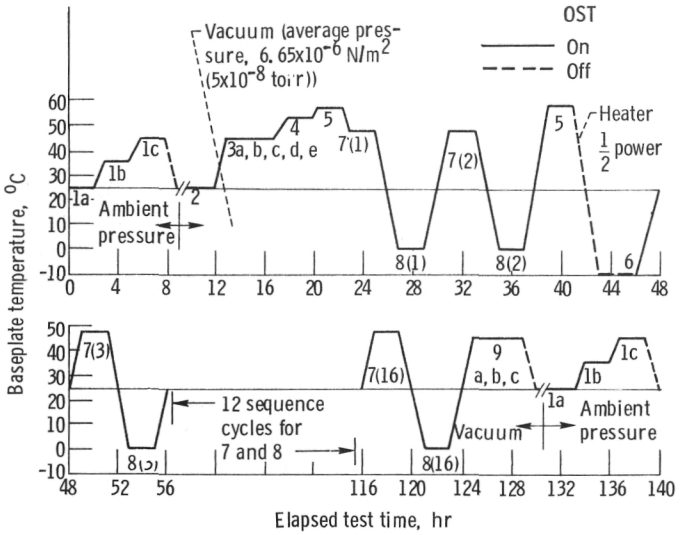

Test and step	OST baseplate temperature, °C	OST operating frequency, GHz	OST drive level
1a	25	12.080	Saturation
b	35		
c	45		
2	25		
3a	45		Zero (dc beam)
b			Saturation
c			6-dB overdrive
d		12.123	Saturation
e		12.038	
4	53	12.080	
5	58		
6	-10		Off (heater ½ power)
7	48		Saturation
8	0		Zero (dc beam)
9a	45		Zero (dc beam)
b	45		Saturation
c	45		6-dB overdrive

(b) Postvibration test sequence. (Cycle number appears in parenthesis following test number.)

Figure 8. - Thermal vacuum testing schedule for CTS OST 2025.

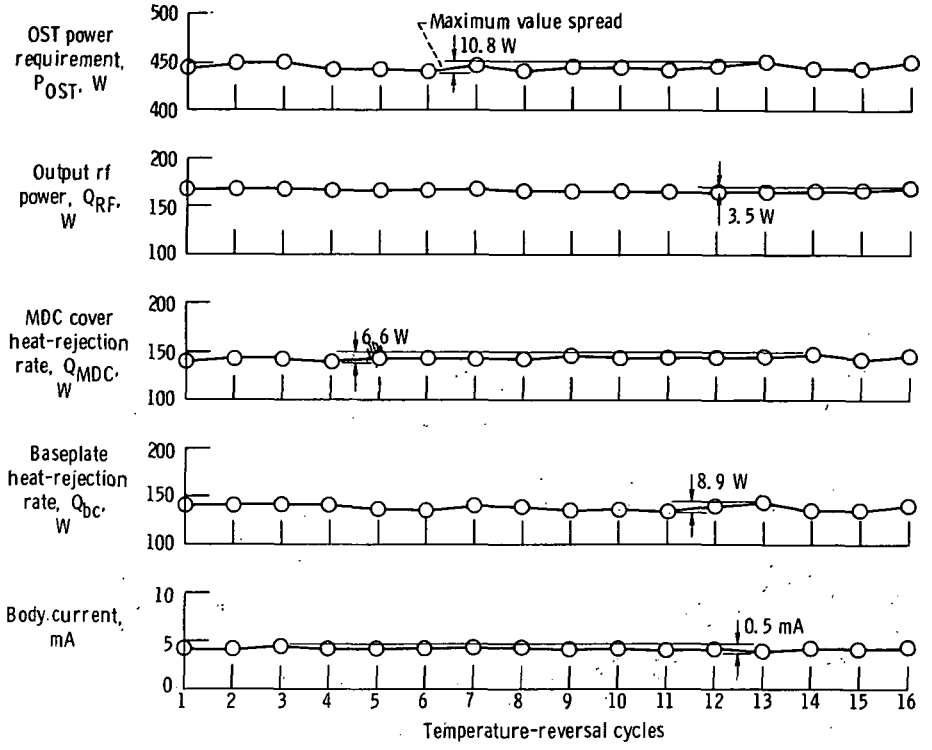

Figure 9. - Variations of experimentally determined characteristics of CTS OST 2025 during temperature-reversal cycle testing. Operating conditions, saturated rf output power condition at center-band frequency and 48° C baseplate temperature.

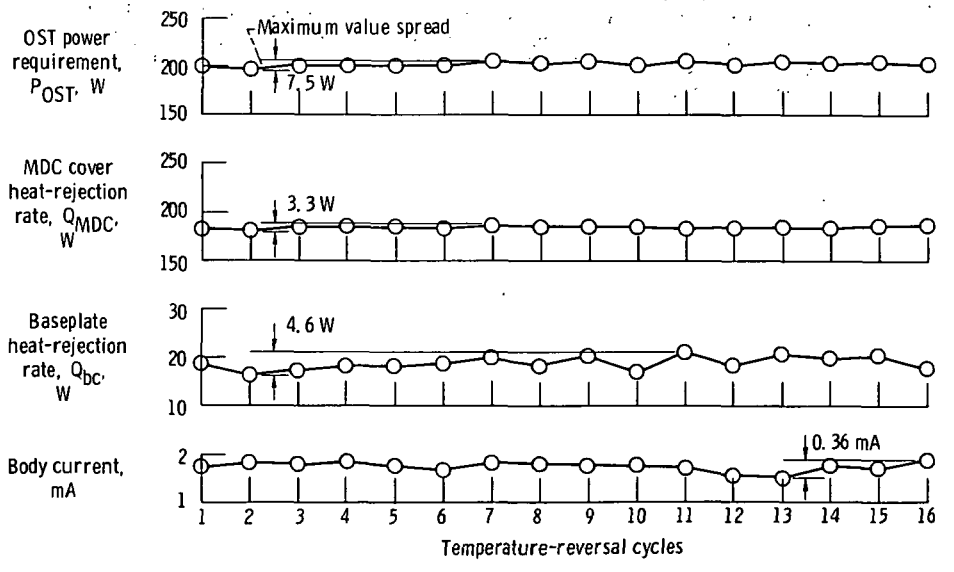

Figure 10. - Variations of experimentally determined characteristics of CTS OST 2025 during temperature-reversal cycle testing. Operating conditions, zero rf output power (dc beam) condition at 0° C baseplate temperature.

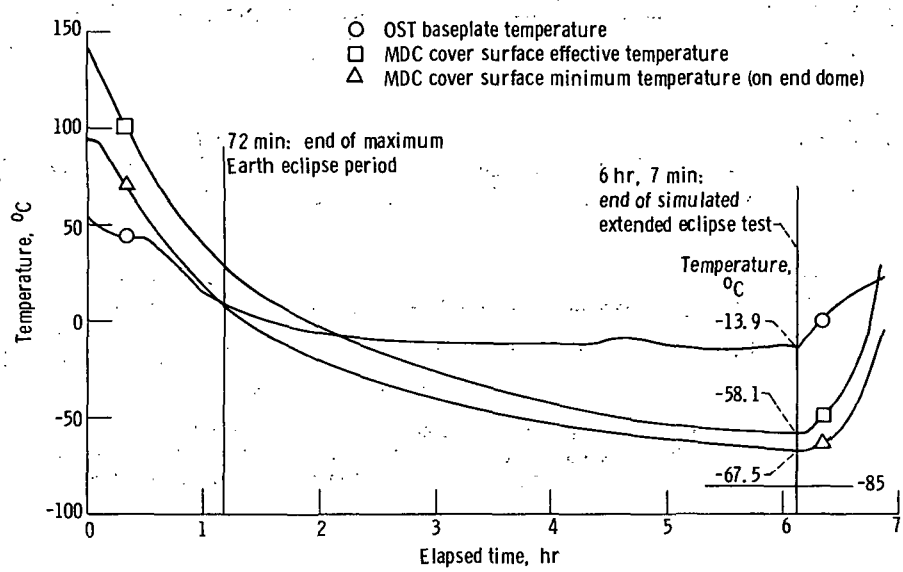

Figure 11. - MDC cover surface temperature in simulated extended eclipse test (postvibration test sequence). Time 0: OST baseplate temperature 54.6° C (equilibrium); saturated rf output power at center-band frequency. Time 0+ to 6 hours, 7 minutes: OST off, cathode heater at 50 percent power. Time 6 hours, 7 minutes: saturated OST rf output power at center-band frequency.

1. Report No. NASA TP-1344	2. Government Accession No.	3. Recipient's Catalog No.
4. Title and Subtitle THERMAL CHARACTERISTICS OF THE 12-GIGAHERTZ, 200-WATT OUTPUT STAGE TUBE FOR THE COMMUNICATIONS TECHNOLOGY SATELLITE		5. Report Date October 1978 6. Performing Organization Code
7. Author(s) Arthur N. Curren		8. Performing Organization Report No. E-9560 10. Work Unit No. 610-22 11. Contract or Grant No.
9. Performing Organization Name and Address National Aeronautics and Space Administration Lewis Research Center Cleveland, Ohio 44135		13. Type of Report and Period Covered Technical Paper
12. Sponsoring Agency Name and Address National Aeronautics and Space Administration Washington, D. C. 20546		14. Sponsoring Agency Code
15. Supplementary Notes		

16. Abstract

A description of the methods used to measure component temperatures and heat-rejection rates in a simulated space environment on candidate output stage tubes (OST's) developed for the Communications Technology Satellite is presented along with summaries of experimentally determined values. The OST's were operated over the entire anticipated operating drive range, from the dc beam (zero drive) condition to the 6-dB overdrive condition. The baseplate temperature was varied from -10° to 58° C with emphasis placed on the testing done at 45° C, the normal anticipated operating temperature. The heat-rejection rate of the OST baseplate ranged from 7.6 W at the dc beam condition to 184.5 W at the 6-dB overdrive condition; the heat-rejection rate of the multistage depressed collector (MDC) cover ranged from 192.2 to 155.9 W for the same conditions. The maximum OST temperature measured on the MDC cover was 227° C during a dc beam test. The minimum temperature measured, also on the MDC cover, was -67.5° C at the end of an extended simulated eclipse test period. No effects were observed on the OST thermal characteristics due to vibration testing or temperature-reversal cycle testing.

17. Key Words (Suggested by Author(s))	18. Distribution Statement
Traveling-wave tube; Heat transfer; Microwave; Communications; Spacecraft	Unclassified - unlimited STAR Category 17

19. Security Classif. (of this report)	20. Security Classif. (of this page)	21. No. of Pages	22. Price*
Unclassified	Unclassified	37	A03

* For sale by the National Technical Information Service, Springfield, Virginia 22161

NASA-Langley, 1978

National Aeronautics and
Space Administration

Washington, D.C.
20546

Official Business
Penalty for Private Use, $300

THIRD-CLASS BULK RATE

Postage and Fees Paid
National Aeronautics and
Space Administration
NASA-451

NASA

POSTMASTER: If Undeliverable (Section 158 Postal Manual) Do Not Return